RESEARCH ARTICLE

NANO · MICRO small
www.small-journal.com

Intrinsically Stretchable Organic Thermoelectric Polymers Enabled by Incorporating Fused-Ring Conjugated Breakers

Chi-Chun Tseng, Kuang-Chieh Wang, Po-Shen Lin, Chi Chang, Li-Lun Yeh, Shih-Huang Tung, Cheng-Liang Liu, and Yen-Ju Cheng**

While research on organic thermoelectric polymers is making significant progress in recent years, realization of a single polymer material possessing both thermoelectric properties and stretchability for the next generation of self-powered wearable electronics is a challenging task and remains an area yet to be explored. A new molecular engineering concept of "conjugated breaker" is employed to impart stretchability to a highly crystalline diketopyrrolepyrrole (DPP)-based polymer. A hexacyclic diindenothieno[2,3-*b*]thiophene (DITT) unit, with two 4-octyloxyphenyl groups substituted at the tetrahedral sp3-carbon bridges, is selected to function as the conjugated breaker that can sterically hinder intermolecular packing to reduce polymers' crystallinity. A series of donor–acceptor random copolymers is thus developed via polymerizing the crystalline DPP units with the DITT conjugated breakers. By controlling the monomeric DPP/DITT ratios, DITT30 reaches the optimal balance of crystalline/amorphous regions, exhibiting an exceptional power factor (PF) value up to 12.5 μW m^{-1} K^{-2} after $FeCl_3$-doping; while, simultaneously displaying the capability to withstand strains exceeding 100%. More significantly, the doped DITT30 film possesses excellent mechanical endurance, retaining 80% of its initial PF value after 200 cycles of stretching/releasing at a strain of 50%. This research marks a pioneering achievement in creating intrinsically stretchable polymers with exceptional thermoelectric properties.

1. Introduction

Thermoelectric materials (TEs) capable of converting thermal energy into electricity through the Seebeck/Peltier effects have emerged as a new green technology.[1] The performance of TEs can be quantified by the power factor (PF) = $S^2\sigma$, where S represents the Seebeck coefficient and σ is conductivity. Inorganic TEs (ITEs) have been widely used in various applications and one of the most appealing and promising applications of TEs is their integration into emergent wearable electronics, such as medical implants or sensors, which enables the generation of electrical power from temperature differences within the human body, thereby reducing the reliance on conventional batteries.[2] Nonetheless, ITEs that often employ rare elements such as lead or tellurium encounter challenges in the context of wearable electronics due to toxicity concerns and a lack of mechanical flexibility.[3] Conversely, organic thermoelectric materials (OTEs) have attracted growing attention in recent years due to the intrinsic benefits of organic semiconductors such as light weight, solution processability, and chemical versatility.[4] Organic materials also possess inherently low thermal conductivity, which is advantageous for achieving notable TE performance.[5] The major superiority of OTEs over ITEs is their capacity to impart mechanical flexibility, bendability, and stretchability.[6] This characteristic opens up opportunities for innovative designs in wearable technologies. Diketopyrrolepyrrole (DPP)-based

C.-C. Tseng, C. Chang, L.-L. Yeh, Y.-J. Cheng
Department of Applied Chemistry
National Yang Ming Chiao Tung University
Hsinchu 30010, Taiwan
E-mail: yjcheng@nycu.edu.tw

The ORCID identification number(s) for the author(s) of this article can be found under https://doi.org/10.1002/smll.202401966

DOI: 10.1002/smll.202401966

K.-C. Wang, P.-S. Lin, C.-L. Liu
Department of Materials Science and Engineering
National Taiwan University
Taipei 10617, Taiwan
E-mail: liucl@ntu.edu.tw

S.-H. Tung
Institute of Polymer Science and Engineering
National Taiwan University
Taipei 10617, Taiwan

C.-L. Liu
Advanced Research Center of Green Materials Science and Technology
National Taiwan University
Taipei 10617, Taiwan

Y.-J. Cheng
Center for Emergent Functional Matter Science
National Yang Ming Chiao Tung University
Hsinchu 30010, Taiwan

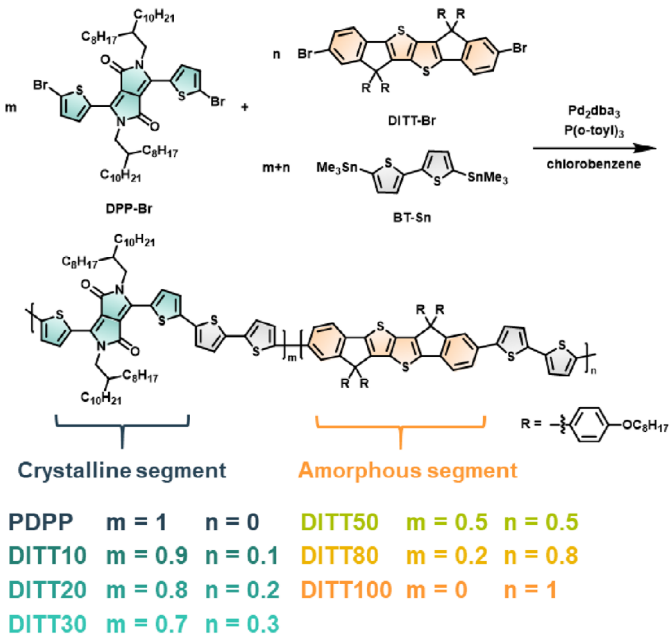

Figure 1. Design of intrinsically stretchable thermoelectric polymers by incorporating a) non-conjugated breakers and b) conjugated breakers.

materials have shown excellent charge carrier mobilities in organic field-effect transistors (OFETs).[7] This is primarily attributed to the polar and coplanar structure of the bicyclic DPP moiety embedded with an endocyclic 1,3-diene, which induces the formation of highly ordered molecular packing structures. Although DPP-based donor–acceptor copolymers have also been employed in organic thermoelectric devices (OTEs), the DPP-based donor–acceptor (D–A) copolymers typically exhibit a high degree of crystallinity, resulting in a rigid and brittle morphology in the resulting thin films.[8] This inherent stiffness makes them inapplicable to self-powered wearable electronics, where mechanical flexibility is essential. Although various molecular engineering strategies have been developed to realize stretchable polymers for OFETs[9] and organic photovoltaics,[10] inherently stretchable organic thermoelectric polymers have not been well explored. For instance, the incorporation of hydrogen bonds or metal–ligand coordination bonds in the polymers introduces additional mechanisms for strain release through the reversible bond breakage.[11] Nevertheless, the existence of hydrogen bonding may give rise to charge traps, adversely affecting charge transport. In addition, the presence of dynamic coordination bonding may detrimentally influence the arrangement of molecular packing, thereby impacting charge mobility. A straightforward method for creating intrinsically stretchable organic thermoelectric (IS-OTE) polymers is to introduce non-conjugated breakers, that is, aliphatic breakers, into the polymer backbone.[12] This approach can indeed impart the material's stretchability, but it typically comes at the cost of reduced charge mobility due to the disruption of conjugation along the polymer backbone (**Figure 1a**). Another strategy involves incorporating fused-ring conjugated breakers that can increase the amorphous portion of the resulting polymers, which helps in dissipating strain when subjected to mechanical forces (Figure 1b).[13] We have designed and synthesized a multifused hexacyclic diindenothieno[2,3-*b*]thiophene (DITT) unit, where a central thieno[2,3-*b*]thiophene (TT) ring was connected to two outer benzene rings through two embedded cyclopentadienyl (CP) rings.[14] The two 4-octyloxyphenyl side chains substituted at the tetrahedral sp^3-carbon bridges within the CP rings extended out of the conjugated plane to effectively prevent strong intermolecular packing (Figure S1, Supporting Information), thereby sterically reducing molecular crystallinity.[15] Although integration of the fused-ring DITT units increased the amorphous characteristics of polymers, its inherently rigid and coplanar conjugated structure enabled it to maintain efficient intrachain charge transport, even within the amorphous region.[16] By introducing DITT and DPP moieties into a polymer with controlled monomeric ratios, the proportions of amorphous and crystalline regions of the resulting polymers could be carefully modulated. This approach could realize intrinsically stretchable polymers; while, exhibiting reasonably high thermoelectric performance. To this end, we selected dibrominated DPP-Br (*m*%, molar fraction) as an acceptor, dibrominated DITT-Br as a donor (*n*%), and distanylated bithiophene (BT-Sn) as a π-bridge ($m + n = 100\%$) for Stille copolymerization. By varying the DITT contents (*n*%) ranging from 0%, 10%, 20%, 30%, 50%, 80%, and 100% relative to the DPP unit, seven random copolymers had been prepared and denoted as PDPP, DITT10, DITT20, PDITT30, DITT50, DITT80, and DITT100, respectively, as shown in **Scheme 1**; Table S1, Supporting Information. Grazing incidence wide-angle X-ray scattering (GIWAXS) demonstrated that the introduction of fused-ring conjugated breakers indeed effectively reduced the crystallinity of the polymer thin films. After sequential doping process, DITT30 could achieve a large PF of 12.5 $\mu W\ m^{-1}\ K^{-2}$ with unprecedentedly high crack onset strain over 100%. DITT30 maintained 80% of original PF value at a strain of 50% after 200 stretch-and-release cycles. To the best of our knowledge, this is the first report of inherently stretchable organic thermoelectric polymers, accomplished by

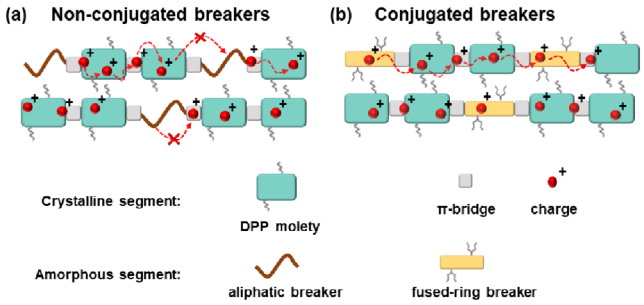

Scheme 1. Synthesis of PDPP/DITT random copolymers by the Stille Coupling Reaction.

integrating fused-ring conjugated breakers. This approach holds substantial promise in broadening the applicability of organic thermoelectric materials in wearable electronics.

2. Results and Discussion

2.1. Synthesis and Characterization of the Polymers

The synthetic route for PDPP/DITT polymers is shown in **Scheme 1**, Supporting Information, and the detailed synthetic procedures and molecular properties are summarized in Table S2, Supporting Information and Supporting Information. The DITT-incorporated polymers were synthesized by Stille polymerization of three monomers using tris(dibenzylideneacetone)dipalladium (Pd_2dba_3) as the catalyst and tris(o-tolyl)phosphine ($P(o\text{-}tol)_3$) as the ligand. The polymers were well characterized by the high-temperature gel permeation chromatography (HT-GPC), high-temperature nuclear magnetic resonance (HT-^{1}H-NMR), and the elemental analysis (EA) measurements (Figures S2–S9 and Table S2, Supporting Information). Upon examining the high-temperature-1H-NMR spectra from PDPP to PDITT10, PDITT20, PDITT30, PDITT50, PDITT80, and PDITT100, we observed a decrease in the integration of protons (4.06 ppm) on the first carbon attached to the nitrogen in the DPP unit, accompanied by an increase in the integration of protons (3.98 ppm) on the first carbon attached to the oxygen in the DITT unit (Figure S9, Supporting Information). Besides, the proton intensity (8.93 ppm) of the thiophene adjacent to the DPP also gradually decreased. Similarly, the content of nitrogen in the polymers progressively decreased in the elemental analysis. These results confirmed the random D–A copolymers with different monomeric ratios were successfully synthesized. To elucidate the electrochemical properties, the highest occupied molecular orbital (HOMO) of DITT-series polymers was evaluated by cyclic voltammetry (CV), as shown in Figure S10 and Table S2, Supporting Information. With increasing the ratio of DITT unit in the random copolymers, the HOMO energy level downshifted from −5.33 to −5.55 eV. The thermal properties of the polymers were investigated by thermogravimetric analysis (TGA) and differential scanning calorimetry (DSC), as shown in Figures S11 and S12, Supporting Information. These polymers exhibited comparable decomposition temperatures (T_d) > 400 °C (at 5% weight loss in the TGA measurements, Figure S11 and Table S2, Supporting Information). For the DSC measurements, PDPP and DITT10 (Figure S12, Supporting Information) showed endothermic melting points at 300 °C and 280 °C upon heating and exothermic crystallization peaks at 278 °C and 170 °C upon cooling, respectively. As for other polymers with increasing DITT contents, no thermal transition peaks were observed within the accessible temperature range, demonstrating that incorporation of DITT reduces the crystallinity of the polymers.

UV–vis–NIR spectroscopy was utilized to elucidate the optical characteristics of PDPP/DITT random copolymer films. The normalized absorption spectra in chlorobenzene and thin film are shown in Figures S13 and S14 and Table S2, Supporting Information. The PDPP exhibited the most red-shifted absorption maxima (λ_{max}) at 780 nm as a result of the strong photo-induced intramolecular charge transfer (ICT) occurring from the tetra-thiophene units to the DPP acceptor units. With an increasing proportion of DITT relative to DPP in copolymers, a gradual blue-shift occurred, which could be attributed to the attenuated ICT effect.[17] Meanwhile, there was a progressive emergence of a distinct absorption peak in the range of 445 to 480 nm, corresponding to the π–π transition of the DITT units. It is interesting to note that PDPP/DITT10 with a high content of DPP, and DITT80/DITT100 with a high content of DITT, had very small $\Delta\lambda_{max}$ values from the solution to the thin film states. This suggests that PDPP and DITT10 likely had strong interactions in both solution and solid state; while, conversely, DITT80 and DITT100 appeared to have weak interactions in both solution and solid states. In contrast, DITT20, DITT30, and DITT50 with more balance DPP/DITT ratios showed a more pronounced $\Delta\lambda_{max}$ from the solution to solid states. This indicates that they have weaker interactions in the solution state than PDPP but tend to aggregate more in the solid state than DITT100. This result demonstrates that by adjusting the DPP/DITT ratios, it is possible to precisely control the crystalline and amorphous properties of polymers through the modulation of intermolecular interactions.

2.2. Characterization of the Doped Polymer Films

All the polymers can be readily doped by $FeCl_3$ and exhibit high carrier concentration (n) and conductivity (σ). The level of doping for each copolymer is systematically controlled by varying the sequential doping duration (1, 3, 5, and 10 s). The doped copolymer films display intensified absorption in the near-infrared region compared to their undoped states, which can be attributed to the polaron or bipolaron transitions arising from the presence of additional charge carriers in the doped copolymer structure (**Figure 2**; Figure S15, Supporting Information).[18] As the doping time increases, the peaks associated with the neutral copolymer in the wavelength range of 500 to 800 nm decrease; while, the peaks associated with the oxidized copolymer in the range of 1000 to 2000 nm increase in all $FeCl_3$-doped copolymer films. Notably, the doping process reaches saturation at a $FeCl_3$ sequential doping time of 5 s. Beyond this threshold, further prolonging the doping time does not yield significant changes in the absorption properties of the doped copolymer films. Therefore, the subsequent analyses in this study are carried out under the 5 s doping time in a 10 mg mL^{-1} $FeCl_3$/acetonitrile solution.

X-ray photoelectron spectroscopy (XPS) is employed to investigate the changes in chemical composition and electronic states

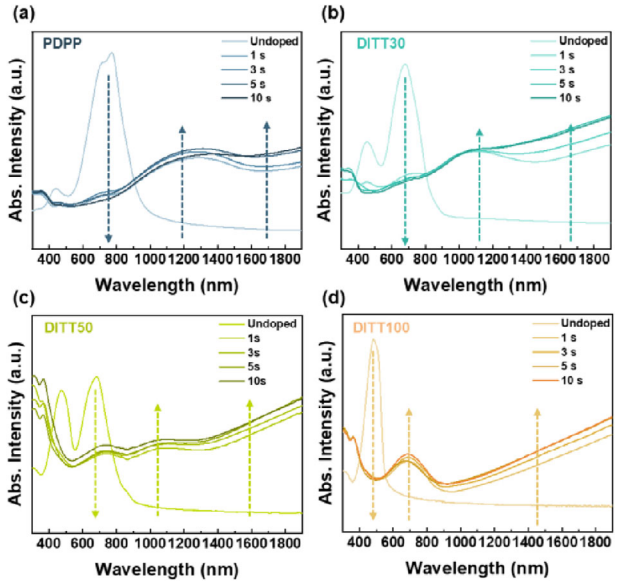

Figure 2. UV–vis–NIR absorbance spectra for undoped and doped a) PDPP, b) DITT30, c) DITT50, and d) DITT100 films.

of the random conjugated copolymer films, both prior to and after the doping process with $FeCl_3$. The XPS findings for the doped copolymer films reveal the presence of additional peaks corresponding to Cl and Fe in the binding energy range of 196–202 eV and 705–740 eV, respectively.[19] When $FeCl_3$ is dissolved in a solvent, it dissociates into $FeCl_2^+$ ions. These ions then engage with the polymer chain. During this interaction, $FeCl_2^+$ is reduced to $FeCl_2$, simultaneously producing Cl^- anions that become integrated within the polymer structure. **Figure 3**; Figure S16, Supporting Information depict the XPS spectra of all the doped copolymer films. These spectra reveal a broad Cl peak

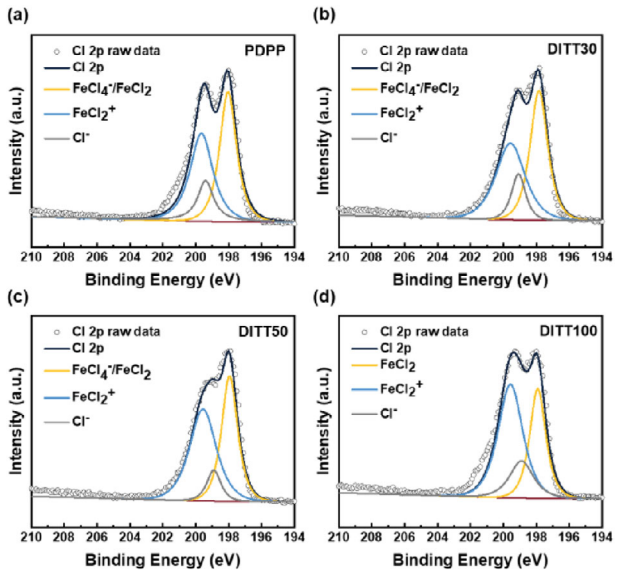

Figure 3. The Cl 2p XPS spectra of $FeCl_3$-doped a) PDPP, b) DITT30, c) DITT50, and d) DITT100 films. The doping efficiency of the polymers was calculated by absorption spectra and XPS.

that can be deconvoluted into three distinct peaks at ≈197, 199, and 200 eV, corresponding to $FeCl_4^-$ and $FeCl_2$ species, Cl^-, and $FeCl_2^+$, respectively. Therefore, the proportion of dopants ionized by charge transfer to the copolymers can be quantified as η_d (doping efficiency), which can be calculated using the following formula:

$$\eta_d = \frac{A^-}{A^0 + A^-} \quad (1)$$

Here, A^- represents the sum of the areas from the Cl^- and $FeCl_2$ species peaks, and A^0 designates the area associated with $FeCl_2^+$ peak. The calculated η_d values for the doped PDPP, DITT10, DITT20, DITT30, DITT50, DITT80, and DITT100 are determined to be 48%, 46%, 45%, 43%, 42%, 37%, and 33%, respectively. These results indicate that random conjugated copolymers with a higher DPP content exhibit the enhanced doping efficiency in generating charge carriers; while, copolymers with a higher DITT content manifest a contrasting trend. Contact angle measurements are utilized to evaluate variations in miscibility between random conjugated copolymer films and the $FeCl_3$/acetonitrile solution, as depicted in Figure S17, Supporting Information. When droplets of the $FeCl_3$/acetonitrile solution are applied to these undoped copolymer films, it is observed that DITT100 exhibits the highest contact angle of 43.1°. In contrast, the contact angles for PDPP, DITT10, DITT20, DITT30, DITT50, and DITT80 are recorded as 30.9°, 32.9°, 38.1°, 38.5°, 41.2°, and 41.2°, respectively. The variations in contact angles of copolymer films reveal that films with a higher proportion of DITT units display a decreased affinity for the $FeCl_3$ solution.[20] This observation suggests that the DITT unit imparts more hydrophobic characteristics to these films, in contrast to the DPP segment containing two sets of polar amide functional groups. Consequently, copolymers with a higher content of the fused rings display lower η_d values due to their reduced miscibility with dopant solution.

2.3. Morphology of the Doped Polymer Films

Atomic force microscopy (AFM) was used to examine the surface morphologies changes of the conjugated random copolymer films both before and after doping process, as depicted in **Figure 4**; Figure S18, Supporting Information. Upon comparing the surface morphologies, it was evident that all copolymer films exhibited similar features of cluster-like structures. However, an increasing ratio of DITT units within the copolymer composition, specifically in the cases of DITT50, DITT80, and DITT100, resulted in a slimmer cluster configuration, as depicted in Figure 4c,d; Figure S18c, Supporting Information. The root-mean-square roughness (R_{rms}) values for undoped PDPP, DITT10, DITT20, DITT30, DITT50, DITT80, and DITT100 were measured at 1.03, 0.51, 0.52, 0.51, 0.39, 0.33, and 0.31 nm, respectively. Subsequent to the sequential doping of copolymer films, doped PDPP, DITT10, DITT20, and DITT30 copolymer films exhibited uniform R_{rms} values of 1.11, 0.49, 0.49, and 0.67 nm, respectively (Figure 4a,b; Figure S18a,b, Supporting Information). However, in the copolymer films with a higher DITT content, the presence of spherical aggregates, indicative of $FeCl_3$ precipitation, was observed in the doped DITT50, DITT80, and DITT100 thin films. This led to a significant increase in the R_{rms} values of

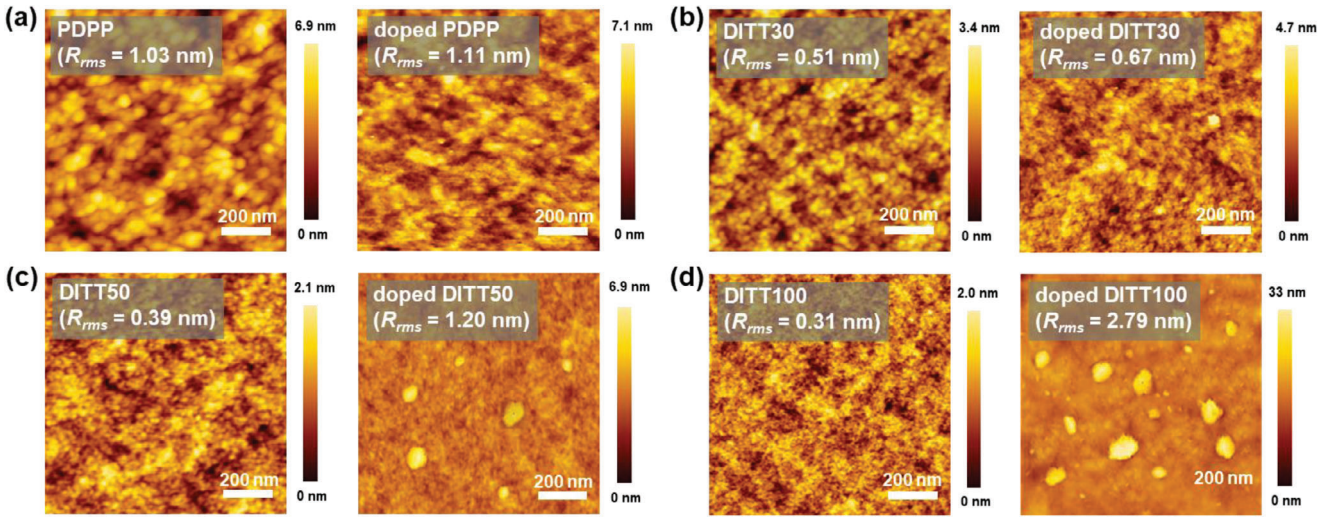

Figure 4. AFM height images of undoped and $FeCl_3$-doped a) PDPP, b) DITT30, c) DITT50, and d) DITT100 polymer films.

1.20, 1.81, and 2.79 nm, respectively, after $FeCl_3$ doping. These phase separations primarily stemmed from the limited miscibility of these copolymers with the $FeCl_3$/acetonitrile solution, hindering the homogeneous incorporation of dopants into the polymer thin films. It is worth noting that this phenomenon may have adverse implications for the mechanical properties of doped copolymer films. Collectively, these observations provide crucial insights into the morphological changes induced by the doping process, underscoring the significant role of polymer composition in the doping procedure.

GIWAXS analysis was employed to investigate the crystalline structures of both undoped and doped random conjugated copolymer films. The GIWAXS patterns of these thin films are illustrated in **Figure 5**; Figure S19, Supporting Information, with the corresponding line-cut profiles presented in Figure S20, Supporting Information. A comprehensive summary of the crystallographic parameters for these films is provided in **Table 1**.

Upon examining the GIWAXS patterns, it is evident that undoped versions of PDPP, DITT10, DITT20, and DITT30 consistently exhibit the (h00) diffraction peaks along the out-of-plane (q_z) direction. This uniformity suggests an edge-on orientation and well-ordered lamellar stacking in their undoped state. In addition, the (010) diffraction peaks are observed in the in-plane (q_{xy}) orientation, corresponding to the parallel π–π, stacking with respect to the substrate in these undoped films. Table 1 summarizes the lamellar spacings of 19.08, 19.03, 19.03, and 18.97 Å and the π–π stacking distances of 3.81, 3.81, 3.85, and 3.87 Å for PDPP, DITT10, DITT20, and DITT30, respectively. Notably, the incorporation of the bulkier DITT unit slightly increases the π–π stacking distances (d_{010}); thus, providing for more space for side-chain interdigitation that leads to the shortened lamellar stacking distances. It should be noted that when the DITT content exceeds 50%, both h_{100} and h_{010} peaks disappear in the undoped DITT50, DITT80, and DITT100 films. The introduction of the DITT unit

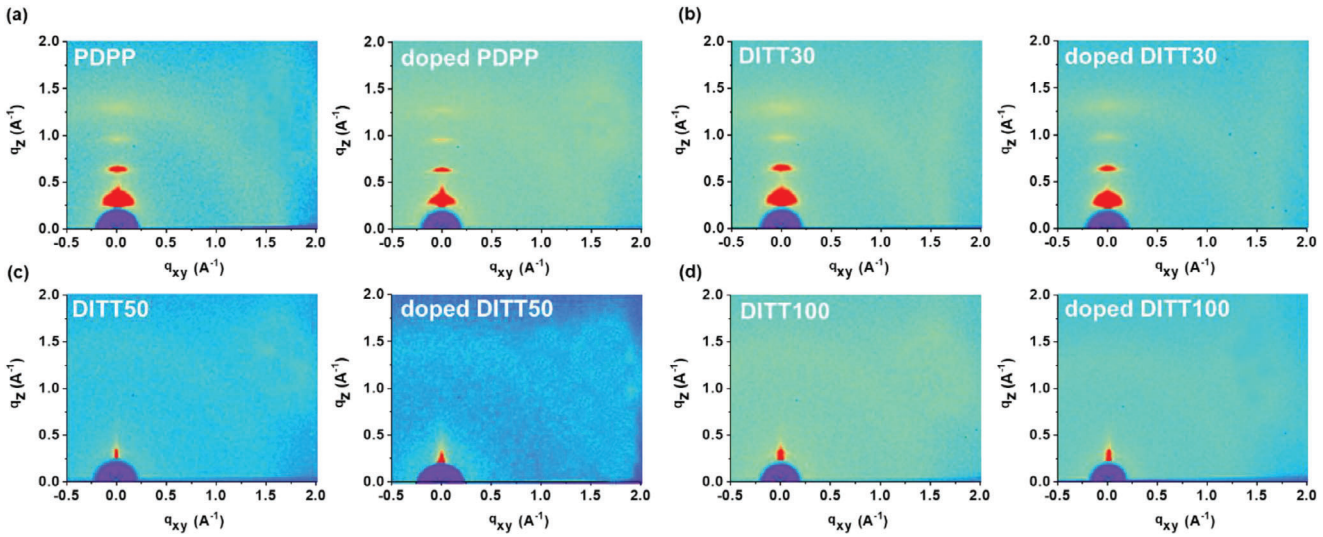

Figure 5. 2D-GIWAXS patterns of undoped and $FeCl_3$-doped a) PDPP, b) DITT30, c) DITT50, and d) DITT100 polymer films.

Table 1. Crystallographic parameters of undoped and $FeCl_3$-doped random conjugated copolymer films.

Sample	Lamellar spacing [Å][a)]	Coherence length [Å][b)]	π–π spacing [Å][c)]	rDoC (100)[d)]
PDPP	19.08	184.7	3.81	1
PDPP (doped)	18.91	202.3	3.83	1.23
DITT10	19.03	178.3	3.81	0.73
DITT10 (doped)	19.00	159.8	3.83	0.37
DITT20	19.03	141.3	3.85	0.51
DITT20 (doped)	18.95	107.4	3.90	0.26
DITT30	18.97	134.1	3.87	0.30
DITT30 (doped)	18.93	101.4	3.88	0.18

[a)] Extracted from fitting the (100) diffraction peak; the stacking distance was calculated by the equation ($d = 2\pi/q$; q represents peak center position); [b)] Calculated based on the lamellar peak FWHM using the Scherrer equation; [c)] Extracted from fitting the (010) diffraction peak; [d)] Extracted from the (100) lamella stacking peak. No clear diffraction peaks were observed in DITT50, DITT80, and DITT100.

into the crystalline domains hinders the conjugated copolymers from forming long-range order due to the bulky groups on the sp^3-carbon of the fused rings, thereby enhancing amorphous characteristics. The relative degrees of crystallinity (rDoC) for the undoped copolymers are determined from the (100) lamellar stacking peak. In comparison to the parent polymer, PDPP, the rDoC values for DITT10, DITT20, and DITT30 are gradually decreased to 73%, 51%, and 30%, respectively. The diffraction patterns of the doped PDPP, DITT10, DITT20, and DITT30 films remain consistent with their undoped counterparts, as detailed in Table 1. This consistency suggests that the doping process does not significantly alter the orientation of the crystalline structure. However, the doping slightly increases the intermolecular d_{010} π–π spacings of PDPP (from 3.81 to 3.83 Å), DITT10 (from 3.81 to 3.83 Å), DITT20 (from 3.85 to 3.90 Å), and DITT30 (from 3.87 to 3.88 Å).

2.4. Thermoelectric Properties of the Doped Polymer Films

The themoelectric properties of the $FeCl_3$-doped copolymer films were evaluated, and the results are summarized in **Figure 6**; Table S3, Supporting Information, showing the variations in the S, σ, and PF. All thermoelectric measurements were conducted at 323 K under a helium atmosphere. It should be noted that all the undoped polymer samples exhibited relatively low σ, rendering the measurement of the S unfeasible. As depicted in Figure 6a, the doped polymer films exhibited σ values of 152 ± 13.6, 84 ± 10.1, 53± 3.2, 38 ± 6.7, 4.2 ± 0.3, 2.6 ± 0.5, and 1.6 ± 0.3 S cm^{-1}, for PDPP, DITT10, DITT20, DITT30, DITT50, DITT80, and DITT100, respectively. PDPP, DITT10, DITT20, and DITT30 exhibited extraordinary σ values, implying that a higher DPP content facilitated charge transport. Carrier mobility (μ) in each $FeCl_3$-doped polymer film was quantified through Hall effect measurements (Figure S21, Supporting Information). From the GIWAXS section mentioned earlier, the doped PDPP displayed the highest rDoC and a μ of 1.87 cm^2 V^{-1} s^{-1}. However, DITT10, DITT20, DITT30, DITT50, DITT80, and DITT100 exhibited significantly reduced μ values of 1.43, 1.14, 0.96, 0.15, 0.12, and 0.009 cm^2 V^{-1} s^{-1}, respectively.[19c] This decrease in μ was more pronounced in DITT50, DITT80, and DITT100, in which the higher DITT content disrupted the polymer's crystalline structure and negatively affected charge transport capabilities. All the $FeCl_3$-doped copolymer films exhibited positive S values, confirming their predominantly p-doping characteristics (Figure 6b). Specifically, PDPP, DITT10, DITT20, DITT30, DITT50, DITT80, and DITT100 exhibited S values of 33.4± 1.1, 40.6 ± 1.8, 45.4 ± 1.2, 57.4 ± 1.5, 67.2 ± 1.4, 87.5 ± 2.2, and 138.4 ± 3.2 μV K^{-1}, respectively. The $FeCl_3$-doped PDPP films demonstrated the highest PF of 16.9 μW m^{-1} K^{-2} (Figure 6c), primarily due to its high σ. The optimized PF values for doped DITT10, DITT20, DITT30, DITT50, DITT80, and DITT100 were 13.9, 11.0, 12.5, 1.1, 2.0, and 3.0 μW m^{-1} K^{-2}, respectively. The relatively low PF value of doped DITT50, DITT80, and DITT100 compared to the other copolymers could be attributed to their poor σ despite high S values.

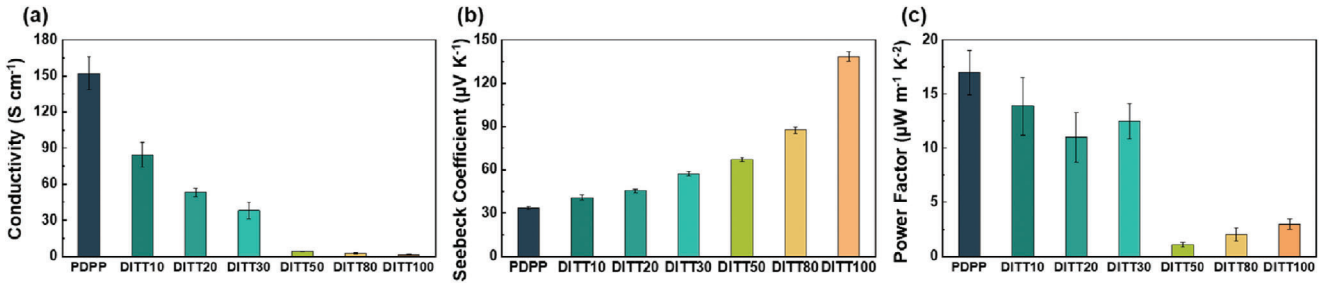

Figure 6. Thermoelectric properties: a) conductivity (σ), b) Seebeck coefficient (S), and c) power factor (PF) of $FeCl_3$-doped polymer films.

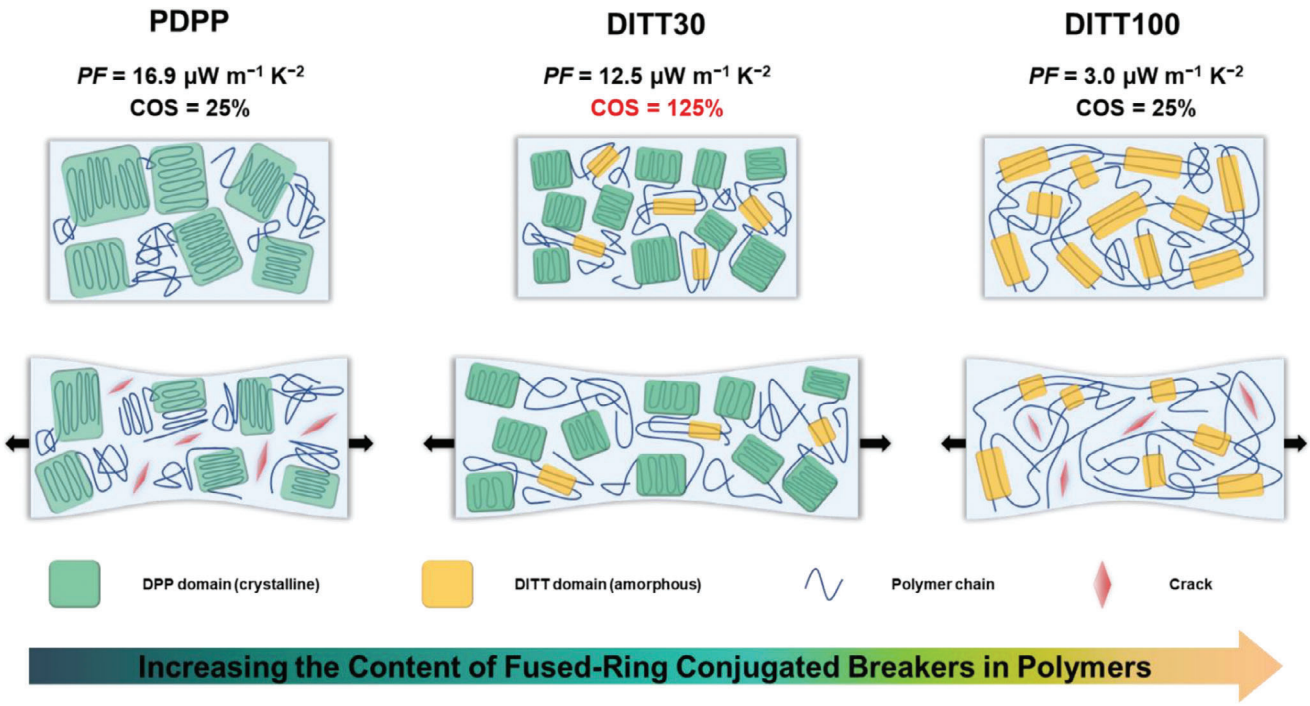

Figure 7. Schematics elucidataion of the effects of fused-ring conjugated breakers on the TE and mechanical properties of PDPP, DITT30, and DITT100.

2.5. Mechanical Properties of the Doped Polymer Films

The investigation of crack onset strain (COS) was conducted to assess the stretchability of the PDPP/DITT copolymers spin-coated on the PDMS substrates. The COS value was monitored by OM images at increasing strains (Figure S22, Supporting Information). In the doped PDPP film, which exhibited minimal stretchability, microscale cracks became visible at ≈25% strain and continued to enlarge as the strain increased. In contrast, DITT10, DITT20, and DITT30 demonstrated significantly enhanced deformability and stretchability, enduring COS of 75%, 100%, and 125%, respectively. This improved stretchability could be attributed to the introduction of the fused-ring conjugated breakers, which provided more amorphous domains capable of releasing stress during stretching. However, DITT50, DITT80, and DITT100 exhibited declined COS values of 50%, 50%, and 25%.

The crystalline structure of the doped copolymer films after strain is further investigated using GIWAXS (Figure S23, Supporting Information). After subjecting the doped DITT10, DITT20, and DITT30 films to tensile strains, the lamellar and π–π distances are slightly increased (Figure S24, Supporting Information) due to the mechanical deformation which may impede the charge carrier transport and increase the resistance within the films.

To comprehend the structure–property relationship, **Figure 7** schematically elucidates the stretching mechanism for PDPP, DITT30, and DITT100. PDPP has the highest content of long-range crystalline domains among the PDPP/DITT polymers, leading to the inherently high PF of 16.9 μW m^{-1} K^{-2}. Nonetheless, the brittleness of the PDPP thin film renders it susceptible to structural damage when subjected to applied strain, resulting in a low COS of 25%. On the other hand, the charge mobility in DITT100 is hampered by the lack of crystalline domains, leading to a moderate PF of 3.0 μW m^{-1} K^{-2}. Unlike traditional aliphatic breakers, DITT, being a conjugated breaker, is relatively bulky and rigid, rendering it difficult to form chain entanglement in the polymer. Consequently, DITT100 polymer also exhibits limited stretchability, with a COS of 25%, due to weaker intermolecular interactions among the conjugated fused-ring DITTs in the enlarged amorphous domains.

Conversely, DITT30 reaches an optimal balance between DPP and DITT units, forming a proportionate mixture of crystalline and amorphous regions with the more flexible copolymer in the amorphous phase working as the tie chains between the crystallites. The amorphous regions are effective in absorbing and dissipating the mechanical stress; while, crystalline regions provide stability to prevent cracking when the force is sustained. Further, the presence of the tie chains connecting adjacent crystallites enhances the ductility and prevents early brittle fracture. As a result, the synergistic effect leads to excellent mechanical stretchability of DITT30 with a COS exceeding 100%. Moreover, the coexistence of short-range crystalline DPP domains and amorphous conjugated DITT domains in DITT30 sustains a high PF of 12.5 μW m^{-1} K^{-2}, overcoming a trade-off between stretchability and OTE performance. These mechanical property measurements indicate that the stretchability of the polymer film can be modulated by incorporating the optimal ratio of the fused-ring conjugated breakers, highlighting the intricate relationship among polymer composition, mechanical properties, and stretchability.

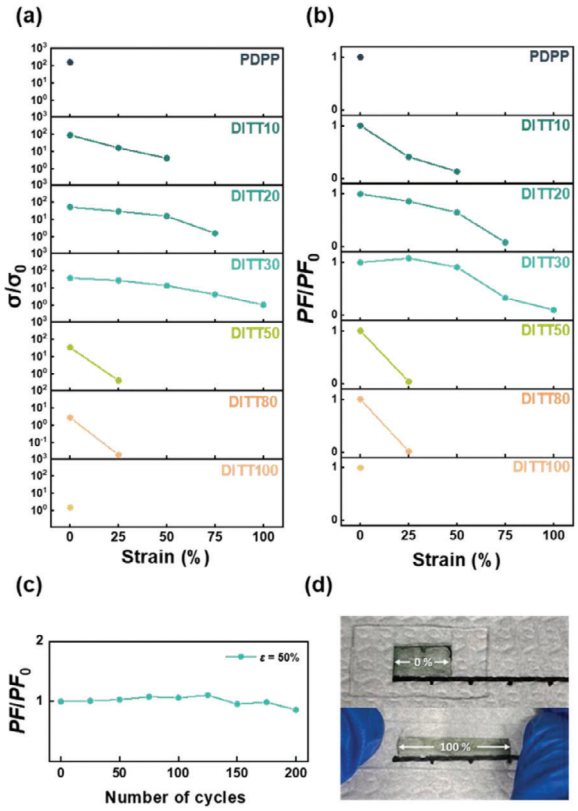

Figure 8. a) σ/σ_0 and b) PF/PF_0 values for the $FeCl_3$-doped polymer films under various tensile strains. c) Plots of PF/PF_0 values under repeated stretch-and-release cycles at a 50% strain. d) Photo of the $FeCl_3$-doped DITT30 thin film before and after 100% strain.

2.6. Strain-Dependent Thermoelectric Properties of the Doped DITT30 Polymer Film

To evaluate the thermoelectric properties of the $FeCl_3$-doped copolymer films under stretching conditions, the doped films on ODTS-treated glass substrates are systematically transferred onto 3M VHB tape and subjected to various strains. **Figure** 8a presents the relative conductivity (σ/σ_0, where σ_0 represents the initial conductivity before strain) of the doped copolymer films measured at different strain levels (0%, 25%, 50%, 75%, and 100%). Figure 8b shows the corresponding relative power factor (PF/PF_0, where PF_0 is the initial power factor before strain) following stretching. It can be observed that the σ/σ_0 values and the PF/PF_0 values decrease with increasing strain. This behavior can be attributed to the formation of small cracks, as shown in the OM images, which has a pronounced effect on charge transport within the films. The maximum strain for the doped PDPP, DITT10, DITT20, DITT30, DITT50, DITT80, and DITT100 copolymer films to maintain the charge transport ability is 0%, 50%, 75%, 100%, 25%, 25%, and 0%, respectively. Notably, the doped DITT30 film demonstrates remarkable performance, retaining 90% of the PF value even under a 50% strain and maintaining its TE properties at strains exceeding 100%.

To access the endurance of the thermoelectric properties, the doped DITT30 film underwent multiple cycles of stretch-and-release at a 50% strain (Figure 8c). Ultimately, the DITT30 film exhibited exceptional durability, retaining 80% of its initial PF after 200 cycles. This indicates that the DITT30 random copolymer could withstand repeated mechanical stretching without significant degradation in its thermoelectric properties. The introduction of DITT unit into the DPP-based polymers improved mechanical stretchability, thereby contributing to the preservation of thermoelectric properties under repeated tensile stretching. Consequently, the utilization of the stretchable DITT30 thin film holds great promise for the development of IS-OTE devices, as depicted in Figure 8d.

3. Conclusion

In this work, we present a new concept of molecular engineering to impart stretchability to highly crystalline DPP-based polymers. In contrast to the typical strategy of incorporating a non-conjugated aliphatic breaker into the polymer main chain, our approach introduces a conjugated fused-ring breaker to reduce crystallinity of the resulting polymer. The C_{2h}-symmetric hexacyclic DITT unit is is chosen to serve as a conjugated breaker of crystallinity. The two bulky 4-octoxyphenyl side chains substituted at the tetrahedral sp^3-carbon bridges in DITT can sterically prevent intermolecular packing, promoting a morphology with more amorphous nanodomains. Meanwhile, the rigid and coplanar fused-ring main chain of DITT ensures the maintenance of high charge mobility in the amorphous region. By polymerizing DPP and DITT monomers in different ratios, a series of random copolymers PDPP, DITT10, DITT20, PDITT30, DITT50, DITT80, and DITT100 is synthesized. The structure–property relationships of all the polymers, including doping efficiency, thin-film morphology, thermoelectric parameters, and mechanical stretchability are thoroughly characterized and elucidated. DITT30 reaches an optimal balance of crystalline/amorphous regions as well as thermoelectric/mechanical properties. The doped DITT30 exhibits a high PF of 12.5 μW m^{-1} K^{-2} due to the coexistence of short-range crystalline DPP domains and amorphous conjugated fused-ring domains. Under stretching conditions, the doped DITT30 film exhibits excellent mechanical stretchability with a strain exceeding 100%, attributed to the synergistic crystalline/amorphous effect. More significantly, the doped DITT30 film exhibits outstanding endurance, retaining 80% of its original TE properties after 200 stretch/release cycles at a strain of 50%. Using conjugated breaker strategy holds great promise of developing IS-OTEs with exceptional thermoelectric properties.

Supporting Information

Supporting Information is available from the Wiley Online Library or from the author.

Acknowledgements

C.-C.T. and K.-C.W. contributed equally to this work. This work was supported by the National Science and Technology Council, Taiwan (grant No. 112-2221-E-A49-002) and Ministry of Education, Taiwan (SPROUT Project-Center for Emergent Functional Matter Science of National Yang Ming

Chiao Tung University). C.-L.L. acknowledges the financial support from the 2030 Cross-Generation Young Scholars Program of the NSTC in Taiwan (grant No. 111-2628-E-002-014 and 112-2628-E-002-013). The authors also thank TLS 13A/17A and TPS 25A at the National Synchrotron Radiation Research Center (NSRRC) of Taiwan for GIWAXS measurements, and Dr. You-Song Cheng at the NYCU Instrumentation Resource Center for the assistance in NMR experiments.

Conflict of Interest

The authors declare no conflict of interest

Data Availability Statement

The data that support the findings of this study are available from the corresponding author upon reasonable request.

Keywords

amorphous segment, doping, fused-ring, organic thermoelectrics, stretchability

Received: March 12, 2024
Revised: April 22, 2024
Published online: May 11, 2024

[1] a) M. Massetti, F. Jiao, A. J. Ferguson, D. Zhao, K. Wijeratne, A. Wurger, J. L. Blackburn, X. Crispin, S. Fabiano, *Chem. Rev.* **2021**, *121*, 12465; b) X. L. Shi, J. Zou, Z. G. Chen, *Chem. Rev.* **2020**, *120*, 7399.

[2] a) C. S. Kim, H. M. Yang, J. Lee, G. S. Lee, H. Choi, Y. J. Kim, S. H. Lim, S. H. Cho, B. J. Cho, *ACS Energy Lett.* **2018**, *3*, 501; b) Y. Zheng, X. Han, J. Yang, Y. Jing, X. Chen, Q. Li, T. Zhang, G. Li, H. Zhu, H. Zhao, G. J. Snyder, K. Zhang, *Energy Environ. Sci.* **2022**, *15*, 2374; c) M. N. Hasan, M. Nafea, N. Nayan, M. S. Mohamed Ali, *Adv. Mater. Technol.* **2021**, *7*, 2101203; d) T. Cao, X. L. Shi, Z. G. Chen, *Prog. Mater. Sci.* **2023**, *131*, 101003.

[3] a) B. S. Kim, G. Lee, H. J. Lim, J. Jang, J. E. Lee, B. K. Min, S. J. Joo, S. Park, B.-k. Ryu, H. S. Lee, *J. Electron. Mater.* **2020**, *49*, 5308; b) S. He, S. Lehmann, A. Bahrami, K. Nielsch, *Adv. Energy Mater.* **2021**, *11*, 2101877.

[4] a) H. Sun, X. Guo, A. Facchetti, *Chem* **2020**, *6*, 1310; b) D. Zhou, H. Zhang, H. Zheng, Z. Xu, H. Xu, H. Guo, P. Li, Y. Tong, B. Hu, L. Chen, *Small* **2022**, *18*, e2200679; c) F. Zhang, C.-a. Di, *Chem. Mater.* **2020**, *32*, 2688; d) N. Pataki, P. Rossi, M. Caironi, *Appl. Phys. Lett.* **2022**, *121*, 230501.

[5] a) J. Tang, Y. H. Pai, Z. Liang, *ACS Energy Lett.* **2022**, *7*, 4299; b) L. Deng, Y. Liu, Y. Zhang, S. Wang, P. Gao, *Adv. Funct. Mater.* **2022**, *33*, 2210770; c) C. Dong, S. Deng, B. Meng, J. Liu, L. Wang, *Angew. Chem., Int. Ed.* **2021**, *60*, 16184; d) J. Han, Y. Jiang, E. Tiernan, C. Ganley, Y. Song, T. Lee, A. Chiu, P. McGuiggan, N. Adams, P. Clancy, T. P. Russell, P. E. Hopkins, S. M. Thon, J. D. Tovar, H. E. Katz, *Angew. Chem., Int. Ed.* **2023**, *62*, e202219313; e) Y. Lu, Z. D. Yu, R. Z. Zhang, Z. F. Yao, H. Y. You, L. Jiang, H. I. Un, B. W. Dong, M. Xiong, J. Y. Wang, J. Pei, *Angew. Chem., Int. Ed.* **2019**, *58*, 11390; f) Y. Shi, J. Li, H. Sun, Y. Li, Y. Wang, Z. Wu, S. Y. Jeong, H. Y. Woo, S. Fabiano, X. Guo, *Angew. Chem., Int. Ed.* **2022**, *61*, e202214192; g) Y. Shi, X. Zhang, T. Du, Y. Han, Y. Deng, Y. Geng, *Angew. Chem., Int. Ed.* **2023**, *62*, e202219262; h) S. Wang, G. Zuo, J. Kim, H. Sirringhaus, *Prog. Polym. Sci.* **2022**, *129*, 101548.

[6] a) Y. Wang, Z. Zhou, J. Zhou, L. Shao, Y. Wang, Y. Deng, *Adv. Energy Mater.* **2021**, *12*, 2102835; b) Y. Zhang, W. Wang, F. Zhang, K. Dai, C. Li, Y. Fan, G. Chen, Q. Zheng, *Small* **2022**, *18*, 2104922; c) S. Xu, X. L. Shi, M. Dargusch, C. Di, J. Zou, Z. G. Chen, *Prog. Mater. Sci.* **2021**, *121*, 100840.

[7] a) C. B. Nielsen, M. Turbiez, I. McCulloch, *Adv. Mater.* **2013**, *25*, 1859; b) X. Zhang, L. J. Richter, D. M. DeLongchamp, R. J. Kline, M. R. Hammond, I. McCulloch, M. Heeney, R. S. Ashraf, J. N. Smith, T. D. Anthopoulos, B. Schroeder, Y. H. Geerts, D. A. Fischer, M. F. Toney, *J. Am. Chem. Soc.* **2011**, *133*, 15073; c) H. W. Lin, W. Y. Lee, W. C. Chen, *J. Mater. Chem.* **2012**, *22*, 2120.

[8] a) I. H. Jung, C. T. Hong, U. H. Lee, Y. H. Kang, K. S. Jang, S. Y. Cho, *Sci. Rep.* **2017**, *7*, 44704; b) J. Ding, Z. Liu, W. Zhao, W. Jin, L. Xiang, Z. Wang, Y. Zeng, Y. Zou, F. Zhang, Y. Yi, Y. Diao, C. R. McNeill, C. A. Di, D. Zhang, D. Zhu, *Angew. Chem., Int. Ed.* **2019**, *58*, 18994; c) Z. Liu, Y. Hu, P. Li, J. Wen, J. He, X. Gao, *J. Mater. Chem. C* **2020**, *8*, 10859.

[9] a) Y. Zheng, S. Zhang, J. B. Tok, Z. Bao, *J. Am. Chem. Soc.* **2022**, *144*, 4699; b) J. Mun, Y. Ochiai, W. Wang, Y. Zheng, Y. Q. Zheng, H. C. Wu, N. Matsuhisa, T. Higashihara, J. B. Tok, Y. Yun, Z. Bao, *Nat. Commun.* **2021**, *12*, 3572; c) J. Meng, J. Dou, Z. Zhou, P. Chen, N. Luo, Y. Li, L. Luo, F. He, H. Geng, X. Shao, H. L. Zhang, Z. Liu, *Angew. Chem., Int. Ed.* **2023**, *62*, e202301863; d) X. Yu, L. Chen, C. Li, C. Gao, X. Xue, X. Zhang, G. Zhang, D. Zhang, *Adv. Mater.* **2023**, *35*, 2209896.

[10] a) Z. Genene, J. W. Lee, S. W. Lee, Q. Chen, Z. Tan, B. A. Abdulahi, D. Yu, T. S. Kim, B. J. Kim, E. Wang, *Adv. Mater.* **2022**, *34*, 2107361; b) J. W. Lee, S. Seo, S. W. Lee, G. U. Kim, S. Han, T. N. Phan, S. Lee, S. Li, T. S. Kim, J. Y. Lee, B. J. Kim, *Adv. Mater.* **2022**, *34*, 2207544; c) S. Seo, J. W. Lee, D. J. Kim, D. Lee, T. N. Phan, J. Park, Z. Tan, S. Cho, T. S. Kim, B. J. Kim, *Adv. Mater.* **2023**, *35*, 2300230; d) J. S. Park, G. U. Kim, S. Lee, J. W. Lee, S. Li, J. Y. Lee, B. J. Kim, *Adv. Mater.* **2022**, *34*, 2201623; e) J. W. Lee, T. N. L. Phan, E. S. Oh, H. G. Lee, T. S. Kim, B. J. Kim, *Adv. Funct. Mater.* **2023**, *33*, 2305851.

[11] a) H. C. Wu, F. Lissel, G. J. N. Wang, D. M. Koshy, S. Nikzad, H. Yan, J. Xu, S. Luo, N. Matsuhisa, Y. Cheng, F. Wang, B. Ji, D. Li, W. C. Chen, G. Xue, Z. Bao, *Adv. Funct. Mater.* **2021**, *31*, 2009201; b) J. Y. Oh, S. Rondeau-Gagne, Y. C. Chiu, A. Chortos, F. Lissel, G. N. Wang, B. C. Schroeder, T. Kurosawa, J. Lopez, T. Katsumata, J. Xu, C. Zhu, X. Gu, W. G. Bae, Y. Kim, L. Jin, J. W. Chung, J. B. Tok, Z. Bao, *Nature* **2016**, *539*, 411; c) Y. Zheng, M. Ashizawa, S. Zhang, J. Kang, S. Nikzad, Z. Yu, Y. Ochiai, H. C. Wu, H. Tran, J. Mun, Y. Q. Zheng, J. B. H. Tok, X. Gu, Z. Bao, *Chem. Mater.* **2020**, *32*, 5700.

[12] a) J. Mun, G. J. N. Wang, J. Y. Oh, T. Katsumata, F. L. Lee, J. Kang, H. C. Wu, F. Lissel, S. Rondeau-Gagné, J. B. H. Tok, Z. Bao, *Adv. Funct. Mater.* **2018**, *28*, 1804222; b) L. A. Galuska, W. W. McNutt, Z. Qian, S. Zhang, D. W. Weller, S. Dhakal, E. R. King, S. E. Morgan, J. D. Azoulay, J. Mei, X. Gu, *Macromolecules* **2020**, *53*, 6032; c) Y. C. Lin, M. Matsuda, C. K. Chen, W. C. Yang, C. C. Chueh, T. Higashihara, W. C. Chen, *Macromolecules* **2021**, *54*, 7388; d) Y. Zhao, X. Zhao, Y. Zang, C.-a. Di, Y. Diao, J. Mei, *Macromolecules* **2015**, *48*, 2048.

[13] a) D. Liu, J. Mun, G. Chen, N. J. Schuster, W. Wang, Y. Zheng, S. Nikzad, J. C. Lai, Y. Wu, D. Zhong, Y. Lin, Y. Lei, Y. Chen, S. Gam, J. W. Chung, Y. Yun, J. B. Tok, Z. Bao, *J. Am. Chem. Soc.* **2021**, *143*, 11679; b) D. Liu, Y. Lei, X. Ji, Y. Wu, Y. Lin, Y. Wang, S. Zhang, Y. Zheng, Y. Chen, J. C. Lai, D. Zhong, H. W. Cheng, J. A. Chiong, X. Gu, S. Gam, Y. Yun, J. B. H. Tok, Z. Bao, *Adv. Funct. Mater.* **2022**, *32*, 2203527

[14] Y. J. Cheng, S. W. Cheng, C. Y. Chang, W. S. Kao, M. H. Liao, C. S. Hsu, *Chem. Commun.* **2012**, *48*, 3203.

[15] a) C. H. Lee, Y. Y. Lai, F. Y. Cao, J. Y. Hsu, Z. L. Lin, U. S. Jeng, C. J. Su, Y. J. Cheng, *J. Mater. Chem. C* **2016**, *4*, 11427; b) W. W. Liang, Y. S. Lin, Y. Y. Lai, Y. J. Cheng, *React. Funct. Polym.* **2016**, *108*, 113; c) J. S. Wu, Y. J. Cheng, M. Dubosc, C. H. Hsieh, C. Y. Chang, C. S. Hsu, *Chem. Commun.* **2010**, *46*, 3259.

[16] J. S. Wu, S. W. Cheng, Y. J. Cheng, C. S. Hsu, *Chem. Soc. Rev.* **2015**, *44*, 1113.
[17] T. Sarkar, S. A. Schneider, G. Ankonina, A. D. Hendsbee, Y. Li, M. F. Toney, G. L. Frey, *Chem. Mater.* **2020**, *32*, 7338.
[18] a) J. Wang, Y. Wang, Q. Li, Z. Li, K. Li, H. Wang, *CCS Chem.* **2021**, *3*, 2482; b) W. Zhao, J. Ding, Y. Zou, C. A. Di, D. Zhu, *Chem. Soc. Rev.* **2020**, *49*, 7210.
[19] a) M. V. Russo, G. Polzonetti, A. Furlani, *Synth. Met.* **1991**, *39*, 291; b) C. H. Tsai, Y. C. Lin, W. N. Wu, S. H. Tung, W. C. Chen, C. L. Liu, *J. Mater. Chem. C* **2023**, *11*, 6874; c) C. Y. Yang, W. L. Jin, J. Wang, Y. F. Ding, S. Nong, K. Shi, Y. Lu, Y. Z. Dai, F. D. Zhuang, T. Lei, C. A. Di, D. Zhu, J. Y. Wang, J. Pei, *Adv. Mater.* **2018**, *30*, 1802850.
[20] D. R Villalva, S. Singh, L. A. Galuska, A. Sharma, J. Han, J. Liu, M. A. Haque, S. Jang, A. H. Emwas, L. J. A. Koster, X. Gu, B. C. Schroeder, D. Baran, *Mater. Horiz.* **2022**, *9*, 500.